Neutron Reflectivity Study of Lipid Membranes Assembled on Ordered Nanocomposite and Nanoporous Silica Thin Films

Dhaval A. Doshi,[†] Andrew M. Dattelbaum,[†] Erik B. Watkins,[†] C. Jeffrey Brinker,[‡,§] Basil I. Swanson,[†] Andrew P. Shreve,[†] Atul N. Parikh,[||] and Jaroslaw Majewski*,[†]

Los Alamos National Laboratory, Los Alamos, New Mexico 87545, Department of Chemical and Nuclear Engineering, University of New Mexico, Albuquerque, New Mexico 87131, Sandia National Laboratories, Albuquerque, New Mexico 87185, and Department of Applied Science, University of California—Davis, Davis, California 95616

Received November 23, 2004. In Final Form: January 13, 2005

Single bilayer membranes of 1-palmitoyl-2-oleoyl-*sn*-glycero-3-phosphocholine (POPC) were formed on ordered nanocomposite and nanoporous silica thin films by fusion of small unilamellar vesicles. The structure of these membranes was investigated using neutron reflectivity. The underlying thin films were formed by evaporation induced self-assembly to obtain periodic arrangements of silica and surfactant molecules in the nanocomposite thin films, followed by photocalcination to oxidatively remove the organics and render the films nanoporous. We show that this platform affords homogeneous and continuous bilayer membranes that have promising applications as model membranes and sensors.

Introduction

Supported lipid membranes find applications in biosensors and are of scientific interest as model biomembranes.[1] Typically, lipid membranes are assembled on supports using Langmuir−Blodgett (LB) deposition or vesicle fusion.[1,2] The assembled membrane is either a single bilayer composed of lipids in each leaflet or a hybrid bilayer where one of the phospholipid leaflets is replaced by an alkylsilane or an alkanethiol covalently attached to the underlying oxide or gold surface, respectively. While the hybrid and supported bilayers exhibit long-term stability, close proximity of the substrate surface gives rise to a number of limitations that hamper many advanced applications of supported membranes in mimicking biological processes. These limitations include localized pinning, frictional drag experienced by the bilayer at the substrate interface, the inability to accommodate many membrane proteins in biologically relevant conformations, and inadequacy in facilitating molecular transport across the membrane plane. In this regard, the use of ultrathin polymeric films as cushions[3,4] or long tethered hydrophilic spacers[5−7] as substrates represent an important step forward. They are expected to reduce bilayer−substrate coupling and also provide an enhanced aqueous phase at the substrate bilayer interface. Recently, gold-coated porous anodic alumina membranes with thiol monolayers have also been used as membrane supports that allow a fluid reservoir and potential single channel addressability.[8−10] However, the presence of a large number of pinning sites that result in defects in the bilayer morphology and impede lateral diffusion detract from the utility of these supports.

An interesting alternative architecture is provided by the use of self-assembled nanoporous or nanostructured silica thin films as supports for phospholipid membranes. In principle, nanocomposite thin films allow encapsulation of functional molecules into the support. Such a construct is attractive for various sensing applications.[11,12] For example, supported membranes can act as selective barriers for electrochemical experiments, and fluorescent molecules trapped within the nanocomposite thin film may be used to detect trans-membrane transport (e.g., ion channel function). Furthermore, the ability of nanoporous films to act as reservoirs of fluids provides the potential of generating architectures with properties closer to those of true biological membranes and may improve the behavior of incorporated trans-membrane proteins. While these constructs hold promise to support membrane architectures with more biologically relevant properties, an important initial step in their application is the thorough characterization of their structure, which is the focus of the present work.

The sensitivity to light elements, nondestructive nature, and long penetration depths of neutrons (compared to X-rays) makes neutron reflectivity (NR) an ideal technique to study the soft and buried membrane−support and membrane−water interfaces. Since neutrons interact with

[†] Los Alamos National Laboratory.
[‡] University of New Mexico.
[§] Sandia National Laboratories.
[||] University of California—Davis.

(1) Sackmann, E. *Science* **1996**, *271*, (5245), 43−48.
(2) Brian, A. A.; McConnell, H. M. *Proc. Natl. Acad. Sci. U.S.A.* **1984**, *81* (19), 6159−6163.
(3) Sackmann, E.; Tanaka, M. *Trends Biotechnol.* **2000**, *18* (2), 58.
(4) Wong, J. Y.; Majewski, J.; Seitz, M.; Park, C. K.; Israelachvili, J. N.; Smith, G. S. *Biophys. J.* **1999**, *77* (3), 1445−57.
(5) Naumann, R.; Schmidt, E. K.; Jonczyk, A.; Fendler, K.; Kadenbach, B.; Liebermann, T.; Offenhausser, A.; Knoll, W. *Biosens. Bioelectron.* **1999**, *14* (7), 651.
(6) Raguse, B.; Braach-Maksvytis, V.; Cornell, B. A.; King, L. G.; Osman, P. D. J.; Pace, R. J.; Wieczorek, L. *Langmuir* **1998**, *14* (3), 648.
(7) Baumgart, T.; Kreiter, M.; Lauer, H.; Naumann, R.; Jung, G.; Jonczyk, A.; Offenhausser, A.; Knoll, W. *J. Colloid Interface Sci.* **2003**, *258* (2), 298.
(8) Drexler, J.; Steinem, C. *J. Phys. Chem. B* **2003**, *107* (40), 11245.
(9) Romer, W.; Steinem, C. *Biophys. J.* **2004**, *86* (2), 955.
(10) Hennesthal, C.; Steinem, C. *J. Am. Chem. Soc.* **2000**, *122* (33), 8085.
(11) Song, X. D.; Nolan, J.; Swanson, B. I. *J. Am. Chem. Soc.* **1998**, *120* (44), 11514.
(12) Song, X. D.; Nolan, J.; Swanson, B. I. *J. Am. Chem. Soc.* **1998**, *120* (19), 4873.

10.1021/la0471240 CCC: $30.25
Published on Web 02/24/2005

the nuclei, isotopic substitution can be exploited to highlight specific parts of the system. Furthermore, light elements, such as deuterium, carbon, nitrogen, and oxygen, strongly scatter neutrons making NR suitable for biological samples. The ability to probe very small sample volumes—on the order of a few nanoliters (10 $cm^2 \times 100$ nm)—by NR is another advantage over other neutron scattering techniques in the study of expensive, rare, or difficult-to-synthesize biomolecules. Recent reviews have discussed the application of NR to address problems in biophysics.[13,14] While specular reflectivity can provide information normal to the solid−liquid or air−liquid interfaces, in-plane inhomogenities and structure can be addressed by studying the off-specular reflection.[15−18] Numerous X-ray and neutron reflectivity studies of model biomembranes have investigated phospholipid monolayers at the air−liquid interface,[19] as well as their interaction with peptides, proteins,[20] and toxins.[21] Supported bilayers have been studied on silicon and quartz substrates as pure phospholipid bilayers[22−25] or hybrid bilayer membranes.[26−29] These studies have reported the structure, surface coverage, and homogeneity of the assembled lipid membranes. In combination with other spectroscopy, microscopy, and scattering techniques, NR is a powerful tool to characterize biological membrane systems.

Ordered nanostructured films are obtained via cooperative self-assembly of amphiphiles (surfactants, block copolymers, lipids) with inorganic sol−gel precursors (silicic acid). An evaporation induced self-assembly (EISA) approach[30] enables deposition of films from solutions, allowing a rich chemistry of the inorganic framework[31] and the ability to spatially pattern structure and composition.[31−34] In this study we have used neutron reflectivity to investigate the structure and the interfacial characteristics of phospholipid membranes on nanocomposite and nanoporous silica thin films. We find that changes of the support surface described by its hydrophobicity and surface charge density affect the lipid membrane structures. These experiments complement other ongoing studies of membrane dynamics within similar types of supported lipid membrane architectures.

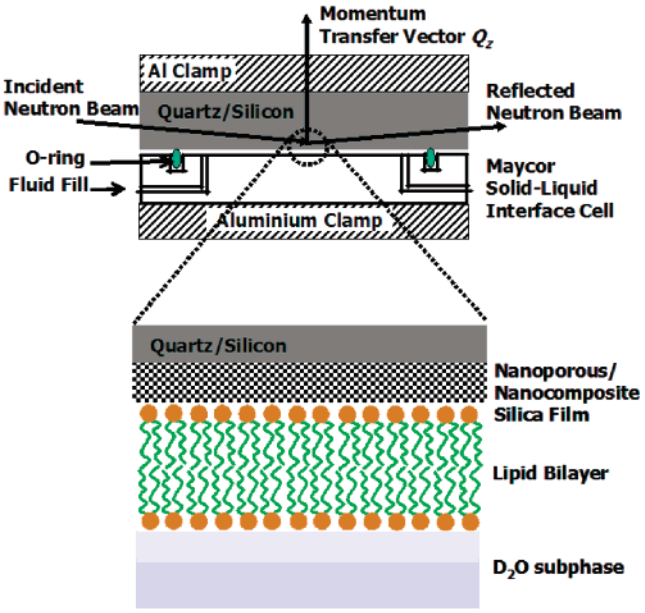

Figure 1. Schematic of the solid−liquid interface cell used for the neutron reflectivity measurements.

Experimental Methods

Materials. POPC was purchased from Avanti Polar Lipids (Alabaster, AL), Brij-56 (polyoxyethylene(10)cetyl ether), TEOS (tetraethoxy silane), deuterated sulfuric acid (D_2SO_4), and D_2O were purchased from Aldrich Chemicals (Milwaukee, WI), and FS-300 ($(CF_2)_n(CH_2CH_2O)_m$; $n \sim 10$, $m \sim 12$) was obtained as a generous gift from DuPont (Wilmington, DE). Silicon wafers of n-type, (111), 75 mm diameter, and 6 mm thickness were purchased from WaferWorld (West Palm Beach, FL). Quartz crystals were purchased from CrysTec (Germany).

Silica Film Preparation. Ordered nanostructured silica thin films were prepared by an EISA approach.[30] Ordered nanocomposite films were spin coated onto 6 mm thick, 75 mm diameter silicon (111) substrates at 2000 rpm for 45 s from a coating sol with a composition (TEOS:FS-300:HCl:H_2O:EtOH = 1:0.1:0.01:7:35) adjusted to generate films in the 800−900 Å thickness range. For the nanoporous films 75 mm × 40 mm × 25 mm quartz crystals were dip coated at 25 mm/s from a coating sol. The coating sol composition, TEOS:Brij-56:HCl:H_2O:EtOH = 1:0.1:0.01:5.2:60, was adjusted to give films in the 200−300 Å range. The surfactant templates were removed by a photocalcination procedure.[35,36] In this process films were exposed to 185−254 nm UV light for about 90 min to ensure complete surfactant removal.[36]

Membrane Preparation. POPC membranes were prepared by vesicle fusion[2] of small unilamellar vesicles that were prepared via an extrusion process.[37] Vesicle fusion was performed in a solid−liquid interface cell (Figure 1) used for neutron reflectivity

(13) Fragneto-Cusani, G. *J. Phys.*: *Condens. Matter* **2001**, *13* (21), 4973−4989.
(14) Krueger, S. *Curr. Opin. Colloid Interface Sci.* **2001**, *6* (2), 111−117.
(15) Munster, C.; Salditt, T.; Vogel, M.; Siebrecht, R.; Peisl, J. *Europhys. Lett.* **1999**, *46* (4), 486−92.
(16) Salditt, T.; Munster, C.; Lu, J.; Vogel, M.; Fenzl, W.; Souvorov, A. *Phys. Rev. E*: *Stat. Phys., Plasmas, Fluids, Relat. Interdiscip. Top.* **1999**, *60* (6), 7285-B.
(17) Sinha, S. K.; Sirota, E. B.; Garoff, S.; Stanley, H. B. *Phys. Rev. B*: *Condens. Matter Mater. Phys.* **1988**, *38* (4), 2297−311.
(18) Pynn, R. *Phys. Rev. B*: *Condens. Matter Mater. Phys.* **1992**, *45* (2), 602−12.
(19) Majewski, J.; Kuhl, T.; Gerstenberg, M.; Israelachvili, J.; Smith, G. *J. Phys. Chem. B* **1997**, *101* (16), 3122−3129.
(20) Kent, M. S.; Yim, H.; Sasaki, D. Y.; Satija, S.; Majewski, J.; Gog, T. *Langmuir* **2004**, *20* (7), 2819−2829.
(21) Miller, C.; Majewski, J.; Faller, R.; Satija, S.; Kuhl, T. *Biophys. J.* **2004**, *86* (6), 3700−08.
(22) Koenig, B.; Kruger, S.; Orts, W.; Majkrzak, C.; Berk, N.; Silverton, J.; Gawrisch, K. *Langmuir* **1996**, *12* (5), 1343−1350.
(23) Fragneto, G.; Graner, F.; Charitat, T.; Dubos, P.; Bellet-Amalric, E. *Langmuir* **2000**, *16* (10), 4581−4588.
(24) Krueger, S.; Ankner, J.; Satija, S.; Majkrzak, C.; Gurley, D.; Colombini, M. *Langmuir* **1995**, *11* (8), 3218−3222.
(25) Burgess, I.; Li, M.; Horswell, S.; Szymanski, G.; Lipkowski, J.; Majewski, J.; Satija, S. *Biophys. J.* **2004**, *86* (3), 1763−1776.
(26) Krueger, S.; Meuse, C.; Majkrzak, C.; Dura, J.; Berk, N.; Tarek, M.; Plant, A. *Langmuir* **2001**, *17* (2), 511−521.
(27) Kuhl, T.; Majewski, J.; Wong, J.; Steinberg, S.; Leckband, D.; Israelachvili, J.; Smith, G. *Biophys. J.* **1998**, *75* (5), 2352−62.
(28) Majkrzak, C.; Berk, N.; Krueger, S.; Dura, J.; Tarek, M.; Tobias, D.; Silin, V.; Meuse, C.; Woodward, J.; Plant, A. *Biophys. J.* **2000**, *79* (6), 3330−40.
(29) Meuse, C.; Krueger, S.; Majkrzak, C.; Dura, J.; Fu, J.; Connor, J.; Plant, A. *Biophys. J.* **1998**, *74* (3), 1388−98.
(30) Brinker, C.; Lu, Y.; Sellinger, A.; Fan, H. *Adv. Mater.* **1999**, *11* (7), 579-+.
(31) Lu, Y.; Fan, H.; Doke, N.; Loy, D.; Assink, R.; LaVan, D.; Brinker, C. *J. Am. Chem. Soc.* **2000**, *122* (22), 5258−5261.
(32) Doshi, D.; Huesing, N.; Lu, M.; Fan, H.; Lu, Y.; Simmons-Potter, K.; Potter, B.; Hurd, A.; Brinker, C. *Science* **2000**, *290* (5489), 107−11.
(33) Fan, H.; Lu, Y.; Stump, A.; Reed, S.; Baer, T.; Schunk, R.; Perez-Luna, V.; Lopez, G.; Brinker, C. *Nature* **2000**, *405* (6782), 56−60.
(34) Dattelbaum, A.; Amweg, M.; Ecke, L.; Yee, C.; Shreve, A.; Parikh, A. *Nano Lett.* **2003**, *3* (6), 719−722.
(35) Clark, T.; Ruiz, J.; Fan, H.; Brinker, C.; Swanson, B.; Parikh, A. *Chem. Mater.* **2000**, *12* (12), 3879−3884.
(36) Dattelbaum, A.; Amweg, M.; Ruiz, J.; Ecke, L.; Shreve, A.; Parikh, A. In *Mechanism of Surfactant Removal From Ordered Nanocomposite Silica Thin Films by Deep-UV Light Exposure*; Materials Research Society Fall Meeting, Boston, MA, 2003; p L7.11.
(37) MacDonald, R. C.; MacDonald, R. I.; Menco, B. P. M.; Takeshita, K.; Subbarao, N. K.; Hu, L. R. *Biochim. Biophys. Acta* **1991**, *1061* (2), 297−303.

measurements. Lipid vesicles in a 10 mM phosphate buffer were kept in contact with the nanocomposite or nanoporous films for 30 min. The cell was then rinsed with a pH 2* D_2O/D_2SO_4 solution (0.01 N D_2SO_4 in D_2O) to remove the excess unattached lipids from the subphase. Neutron reflectivity measurements were performed with a subphase of D_2O at pH 2* (0.01 N D_2SO_4 in D_2O). D_2O at pH 2* was chosen to prevent the dissolution of nanoporous silica thin film as would occur in pH $\approx$ 7 aqueous solutions.[38−40] Dunphy and co-workers (2003) have shown that phosphate buffer stable nanoporous silica films can be prepared by incorporating 2−5% aluminum in the silica matrix. Our control experiments indicate that pH 2 subphase does not adversely affect the lipid bilayer structure and fluidity on the time scale of the neutron experiments (see Supporting Information).

Transmission Electron Microscopy. Transmission electron microscopy (TEM) measurements were performed at Department of Earth and Planetary Sciences, University of New Mexico. A JEOL 2010 operating at an accelerating voltage of 200 kV and equipped with a Gatan slow scan CCD (charged coupled device) camera was used to investigate the structure. Flakes of the thin film were scraped off the silicon substrate with sharp blades and transferred onto a holey carbon TEM grid. Images were acquired at magnifications of 40000−60000.

Neutron Reflectivity. The reflectivity R of a surface is defined as the ratio of the number of particles (neutrons or photons) elastically and specularly scattered from the surface to the number of incident particles. When measured as a function of wave vector transfer (defined below), the reflectivity curve contains information regarding the sample-normal profile of the in-plane average of the coherent scattering cross sections. As will be shown below, the NR yields a profile of the coherent neutron scattering length density (SLD), ρ. If one knows the chemical constituents of the investigated system and knows the SLD distribution, the concentration of a given atomic species at a particular depth can then be calculated. Neutron reflectivity measurements were performed on the SPEAR beamline, a time-of-flight reflectometer, at the Manuel Lujan Neutron Scattering Center, Los Alamos National Laboratory (http://www.lansce.lanl.gov/lujan/index.html). The neutron beam is produced by spallation of neutrons from a tungsten target using a pulsed beam (20 Hz) of 800 MeV protons. A partially coupled liquid hydrogen moderator at 20 K modifies the neutron energy spectrum. Neutrons with wavelengths $\lambda = 2-16$ Å are selected by means of choppers and frame-overlap mirrors (http://www.lansce.lanl.gov/lujan/ER1ER2/SPEAR/index.html). The momentum transfer vector Q_z range, $Q_z = 4\pi \sin(\alpha)/\lambda$ (where α is the angle of incidence measured from the sample surface and λ is the wavelength of the probe), is covered by performing measurements at two angles of incidence, typically 0.5° and 2.5°. The beam footprint was 10 mm × 50 mm. The background limits the Q_z range over which reflectivity data can be collected; scattering from the subphase has a significant contribution to the background. Hence, we designed a cell made of Maycor (Ceramic Products Inc., Palisades Park, NJ, containing SiO_2:MgO:Al_2O_3:K_2O:B_2O_3:F in the weight ratio 46:17:16:10:7:4) to minimize the cell scattering, and the O-ring groove was machined to achieve a subphase reservoir depth of about 50 μm (Figure 1). These enhancements in the sample environment and others in beam intensity and beamline optics allow us to measure reflectivities R, with $R \approx 5 \times 10^{-7}$ and momentum transfer vector Q_z of 0.25−0.3 Å^{-1} in less than 4 h. The data are reduced and plotted as RQ_z^4 versus Q_z to compensate for the sharp decrease in the reflectivity as described by Fresnel's law: $R \propto Q_z^{-4}$.[41]

The intensity of the specular reflectivity and the real space SLD are related by an inverse transformation. Since, as in most scattering experiments, phase information is lost when collecting the specular reflectivity and due to the nonlinear nature of the inverse transformation itself, a unique solution to the problem cannot be obtained analytically. The reflectivity data were analyzed by model independent B-spline profiles[42] and a model-dependent Parratt fitting algorithm. While the model-dependent method requires a priori knowledge of the composition of the sample (SLD profile), the model-independent method has no such requirement. Other model-independent techniques such as the maximum entropy method[43] and sin−cosine series[42] have also been applied for NR data fitting, but these are not considered in this study. Recently, Majkrzak and co-workers have used phase-sensitive NR to determine the SLD profile from first principles with no assumptions attached.[28] The technique requires the ability to change the SLD of one of the layers in the system investigated without affecting the rest of the system; this stringent requirement is not easily fulfilled for all systems of interest.

(i) B-Spline Profiles. The SLD profile of the data is composed of randomly generated smooth functions represented by cubic B-splines,[42,44] also known as parametric B-splines.[42,44,45] Starting from a random B-spline curve, a fitting procedure is applied to obtain B-spline curves that reproduce the measured reflectivity data. The fitting routine requires the user to input the difference in the SLD of the substrate and the subphase, $\Delta\rho$, number of B-splines to use, n, a dampening factor, β, and the distance between the substrate and the subphase, d. For computational optimization, the program used here[42] further employs a function A_1, which determines the smoothness of the solution with a weighting parameter w_1, a biasing function A_2, to bias the solution toward an expected average scattering-length density, and a second weight parameter w_2, which weighs A_1/A_2. Curves with physical relevance to the system are chosen and refined by varying the parameters (β, n, d) to obtain fits that minimize the χ^2.[42,44]

(ii) Box Models. The reflectivity data were analyzed by an optical matrix method using the Parratt formalism.[46] Here our philosophy was to use the simplest possible model of physical relevance. In particular, while knowing that the nanostructured film has a superlattice structure,[47,48] we, however, modeled it with a single box. Deviations of model fits from the data in regions that can be attributed to the film thickness are a result of this simplification. In all cases, the interfacial roughness, σ, was modeled by a Gaussian roughness. From the error analysis ($\chi^2 \rightarrow \chi^{2+1}$) for fit parameters, the error bar on the lipid membrane thickness is of the order of 0.5 Å and 0.05×10^{-6} Å^{-2} on its SLD.

Results and Discussion

Figure 2 shows the TEM micrograph of the ordered nanocomposite film (FS-300 templated) with the organic (surfactant, lighter regions) and inorganic (silica, darker regions) components. The image shows organization of the cylindrical tubules with a d spacing of 43 Å that aligns with the long axis parallel to the Si/quartz substrate. The inset shows the edge view of such a packing arrangement, which is consistent with a hexagonal mesophase (*p6mm* symmetry). While it is well-known,[1] and we observe the same for silanated nanoporous thin films (data not shown), that on hydrophobic surfaces such as self-assembled alkylsilanes or thiol-coated supports a lipid monolayer is formed with its tails in contact with the alkyl chains, it was not initially clear what membrane structure would assemble on the slightly hydrophobic nanocomposite film surface (water contact angle ~40°).

Figure 3a shows the NR data measured for a lipid bilayer membrane fused onto a 835 Å thick nanocomposite silica thin film. For this sample and also for others in this study,

(38) Iler, R. *Chemistry of Silica*; Wiley: New York, 1979.
(39) Brinker, C.; Scherer, G. *Sol−Gel Science*: *The Physics and Chemistry of Sol−Gel Processing*; Academic Press: San Diego, CA, 1990.
(40) Dunphy, D.; Singer, S.; Cook, A.; Smarsly, B.; Doshi, D.; Brinker, C. *Langmuir* **2003**, *19* (24), 10403−10408.
(41) Als-Nielsen, J. *Physica A* **1986**, *140*, 376−389.
(42) Pedersen, J. S.; Hamley, I. W. *J. Appl. Crystallogr.* **1994**, *27*, 36.
(43) Sivia, D. S.; Hamilton, W. A.; Smith, G. S. *Physica B* **1991**, *173* (1/2), 121−38.
(44) Pedersen, J. S.; Hamley, I. W. *Physica B, Int. Conf. Surf. X-ray Neutron Scattering (SXNS-3)* **1994**, *198* (1/3), 16−23.
(45) Berk, N.; Majkrzak, C. *Phys. Rev. B*: *Condens. Matter* **1995**, *51* (17), 11296−11309.
(46) Parratt, L. *Phys. Rev.* **1954**, *95*, 359−369.
(47) Doshi, D.; Gibaud, A.; Goletto, V.; Lu, M.; Gerung, H.; Ocko, B.; Han, S.; Brinker, C. *J. Am. Chem. Soc.* **2003**, *125* (38), 11646−11655.
(48) Gibaud, A.; Baptiste, A.; Doshi, D.; Brinker, C.; Yang, L.; Ocko, B. *Europhys. Lett.* **2003**, *63* (6), 833−839.

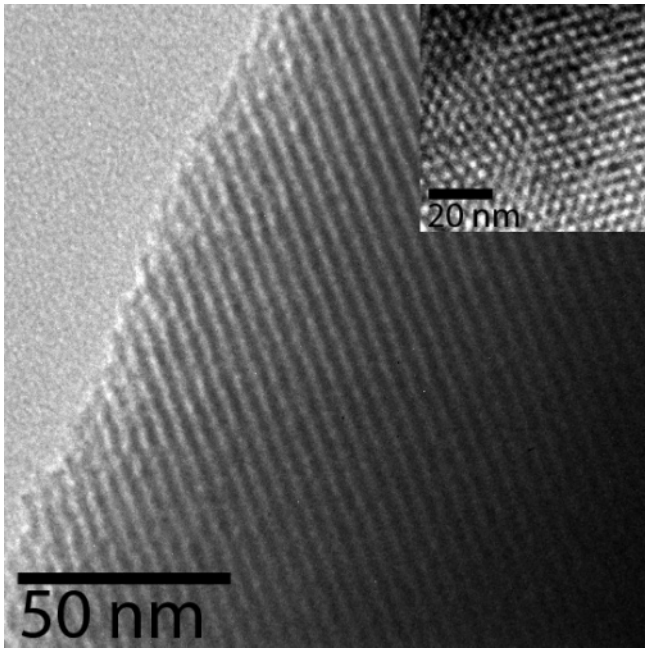

Figure 2. TEM micrograph of the nanocomposite film. Inset shows the edge view of the film revealing the hexagonal packing of cylindrical tubules.

since the footprint of the neutron beam is 50 mm × 10 mm, the efficacy of vesicle fusion is probed on large surface areas as compared to traditional AFM measurements that probe areas of the order of tens of μm^2. Complementary fluorescence recovery after photobleaching (FRAP) studies have demonstrated lateral fluidity of the lipid bilayer membranes supported on nanoporous and nanocomposite films and is the subject of a separate paper. Kiessig fringes with periodicity $\Delta Q_z = 2\pi/t$ arising from the thin-film thickness, t = 835 Å, are clearly visible. Plotting the reflectivity data in RQ_z^4 versus Q_z format allows visual analysis of the smaller length scales present in the measured system. The minimum at $Q_z = 0.19$ Å^{-1} can be attributed to the thickness of the lipid membrane. The data were fit with a two-box model corresponding to the silica thin film and the lipid membrane, represented here by hydrocarbon chains only. The fit parameters are shown in Table 1, and the SLD profile is shown in Figure 3b. We also tried to fit the data including the native silicon dioxide and the lipid headgroup layer as additional boxes. However, this did not improve the fit, which likely reflects the lack of scattering contrast between the native SiO_2 SLD ($\rho_{SiO_2} = 3.47 \times 10^{-6}$ Å^{-2}), the nanocomposite film SLD ($\rho_{\text{nanocomposite film}} = 3.76 \times 10^{-6}$ Å^{-2}), and that of the combined headgroup plus water layer ($\rho_{\text{water cushion+headgroup}} = 3.8 \times 10^{-6}$ Å^{-2} from Table 3). Hence, the thickness of 835 Å includes the contribution from the native SiO_2, nanocomposite film, and the headgroup plus water layer. The lipid headgroups in contact with the acidic D_2O subphase also cannot be resolved due to lack of scattering contrast. Attempts to fit these data with B-splines were also unsuccessful, probably due to the large number of closely spaced interference fringes. The numerical routine used is not optimized for thick films.

The two-box box model fit parameter for the membrane thickness (hydrocarbon tails only), $t_{\text{bilayer,HCtails}} = 33$ Å, clearly suggests that a single bilayer membrane is formed. Further, the SLD of -0.37×10^{-6} Å^{-2} suggests that the membrane is densely packed (note that the SLD for a well-packed monolayer of organic hydrocarbons is $\approx -0.44 \times 10^{-6}$ Å^{-2}). The thickness of a POPC lipid

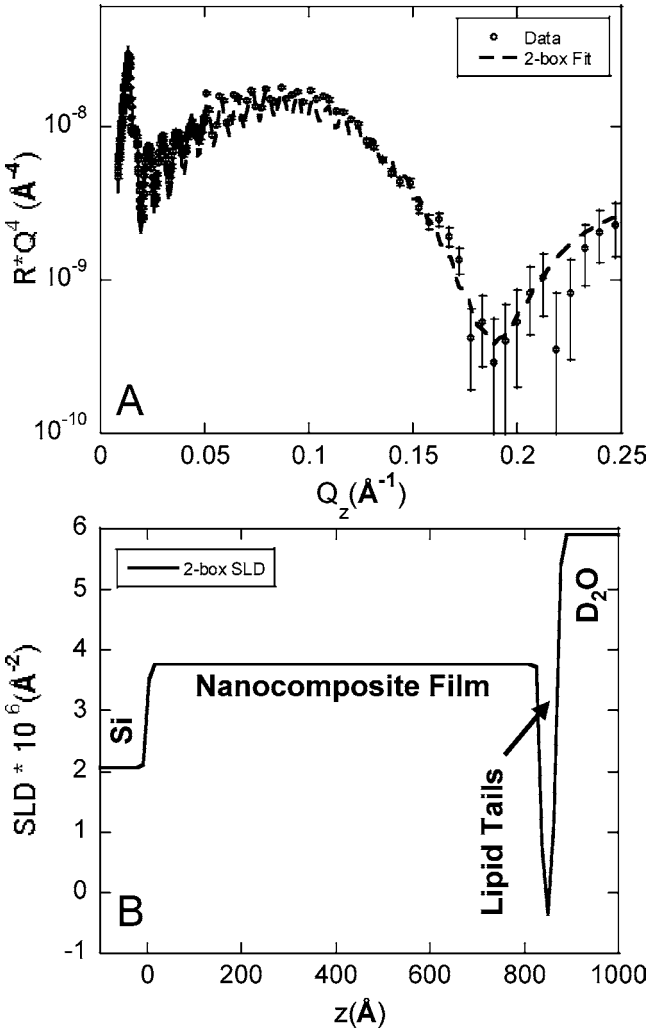

Figure 3. (A) Neutron reflectivity measured for lipid bilayer on a nanocomposite film and the box-model fit based on the SLD profile shown in B. (B) SLD profile for the box model fit in A.

Table 1. Two-Box Model Fit Parameter for Lipid Bilayer on Nanocomposite Silica Thin Film

	t, Å	ρ, Å^{-2} × 10^6	σ, Å
silicon		2.07	
nanocomposite silica film	835	3.76	4.1
lipid bilayer (HC tails)	33.1	−0.37	4.3
subphase		5.91	6.1

Table 2. Two-Box Model Fit Parameter for Lipid Bilayer on Nanoporous Silica Thin Film

	t, Å	ρ, Å^{-2} × 10^6	σ, Å
quartz		4.07	
nanoporous silica film	187	4.77	28
lipid bilayer (HC tails)	37.2	−0.45	4.6
subphase		5.91	9.5

bilayer (hydrocarbon tails) is smaller than expected from molecular dynamics simulations,[49] $t_{\text{bilayer,HCtails}} = 38 \pm 1$ Å, and X-ray reflectivity reports in the literature, $t_{\text{bilayer,HCtails}} = 39$ Å.[50] In general this behavior results from the (i) presence of gauche defects in the leaflets, (ii) tilting of the molecules in the leaflets, or (iii) some interdigitation of the lipid hydrocarbon tails. For lipids in their gel phase,

(49) Pasenkiewicz-Gierula, M.; Murzyn, K.; Rog, T.; Czaplewski, C. *Acta Biochim. Pol.* **2000**, *47* (3), 601.
(50) Vogel, M.; Munster, C.; Fenzl, W.; Salditt, T. *Phys. Rev. Lett.* **2000**, *84* (2), 390−393.

Table 3. Three-Box Model Fit Parameter for Lipid Bilayer on Nanoporous Silica Thin Film

	t, Å	ρ, Å^{-2} × 10^6	σ, Å
quartz		4.07	
nanoporous silica film	187	4.77	28
water cushion including headgroup	14.6	3.80	6.4
lipid bilayer (HC tails)	35.1	−0.40	1.5
subphase		5.91	9.5

tilting of the molecules is used to explain the observation of lower thickness of bilayers. However, in the case of POPC at room temperature the lipids are fluid like (t_{gel} ~ −4 °C); hence the presence of gauche defects and potential interdigitation are more likely explanations. An alternative explanation may be provided by Burgess et al.[25] who found from NR measurements that fluid dimyristoylphosphatidylcholine (DMPC)/cholesterol bilayer thickness decreases to almost half the maximum possible as the surface charge density decreases from −30 to −1 μCcm^{-2}, which they explain by the tilt angle for DMPC lipid membrane increasing from 35° to 60°.

The area per unit molecule for the POPC lipid membrane can also provide some information about how well formed the lipid membrane is on top of the ordered nanocomposite silica thin film. This value can be calculated by combining the thickness and the SLD information. Since the chemical composition of the membrane is known, one can calculate the area using the formulas

$$\mathrm{SLD} = (1/v_m)\Sigma(b_i)$$

$$v_m = A(t_{bilayer}/2)$$

where v_m is the molecular volume (Å^3), the b_i are the bound coherent scattering lengths (Å) ($b_{Carbon} = 6.646 \times 10^{-5}$ Å, $b_{Hydrogen} = -3.739 \times 10^{-5}$ Å), and A is the area per POPC molecule (Å^2). For POPC bilayer hydrocarbon tails ($C_{32}H_{64}$) with a SLD of $(-0.37 \pm 0.05) \times 10^{-6}$Å^{-2} and thickness of 33.1 ± 0.5 Å the calculated area per unit molecule is 44 ± 7 Å^2. This value is lower than the one obtained from surface balance experiments[51] and molecular dynamics simulations[49] of 64−66 Å^2, but the inconsistency might, in part, reflect the uncertainty in the SLD value due to a simplified model used to describe the system. Nevertheless, this value indicates again that the lipid molecules are tightly packed in a well-formed supported lipid bilayer.

Ordered nanoporous silica films were also used to support a lipid membrane architecture. The nanocomposite films described above can be converted into nanoporous films by either photo or thermal calcinations or solvent extraction to remove the surfactant from the supporting film. Consolidation of the siloxane network during photo/thermal calcinations results in a 10−35% shrinkage in the film thickness.[32] Depending on the initial film composition, these procedures can also cause phase transformations into three-dimensional (3D) cubic or 3D hexagonal nanostructures.[32,52] Since the calcination procedure used here to prepare the ordered nanoporous silica thin films results in very hydrophilic films with a water contact angle <10°, it was expected that a single well-formed lipid bilayer would assemble on the surface of the nanoporous thin film.

Figure 4a shows the NR data for a lipid bilayer prepared on a different nanoporous silica thin film. Since the NR

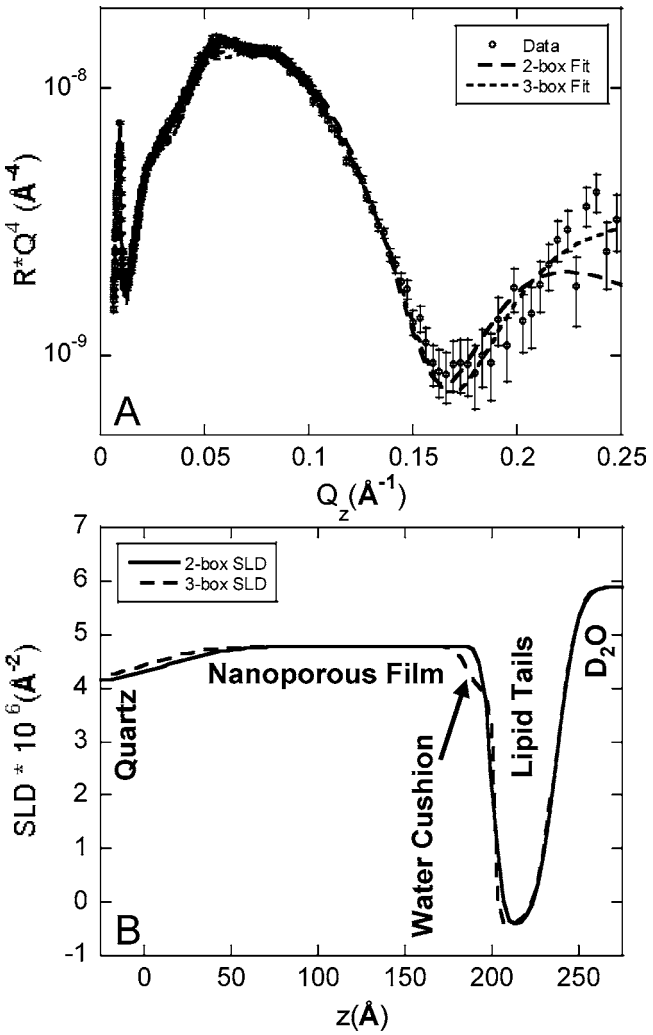

Figure 4. (A) Neutron reflectivity measured for a lipid bilayer on a nanoporous film and the two- and three-box model fit based on the SLD profiles shown in A. (B) SLD profiles for the box model fits in A.

data extends to $Q_{z,max}$ of 0.25 A^{-1}, we have direct evidence (from the position of the minima[53]) of length scales greater than $\pi/Q_{z,max}$ = 12.5 A^{-1}; however, the reflectivity is affected by the presence of smaller length scale layers whose thickness can be determined, indirectly, by model-dependent fitting. Here we have modeled the system with two and three boxes. The additional box describes the hydrated lipid headgroups along with the water cushion layer that is present at the silica film−lipid membrane interface (Table 3). In this system, there is enough SLD contrast to separate out the lipid headgroups along with the water cushion from the nanoporous support, unlike the case of a lipid membrane supported on an ordered nanocomposite silica film. The three-box model gives a lower χ^2 for the fit (34 versus 46) and is supported by the fact that a 10−20 Å water cushion layer is known to exist between hydrophilic solid supports and lipid membranes.[22,54] The fit parameters for the two-box and three-box models are tabulated in Tables 2 and 3, respectively. Figure 4b shows the SLD profile for the two-box and three-box models; the curves start together in the D_2O subphase (z >250 Å) and deviate in the region 175 Å < z < 200 Å,

(51) Hyslop, P. A.; Morel, B.; Sauerheber, R. D. *Biochemistry* **1990**, *29* (4), 1025.
(52) Lu, Y.; Ganguli, R.; Drewien, C.; Anderson, M.; Brinker, C.; Gong, W.; Guo, Y.; Soyez, H.; Dunn, B.; Huang, M.; Zink, J. *Nature* **1997**, *389* (6649), 364−368.
(53) Kjaer, K. *Physica B* **1994**, *198* (1/3), 100.
(54) Johnson, S. J.; Bayerl, T. M.; McDermott, D. C.; Adam, G. W.; Rennie, A. R.; Thomas, R. K.; Sackmann, E. *Biophys. J.* **1991**, *59* (2), 289−94.

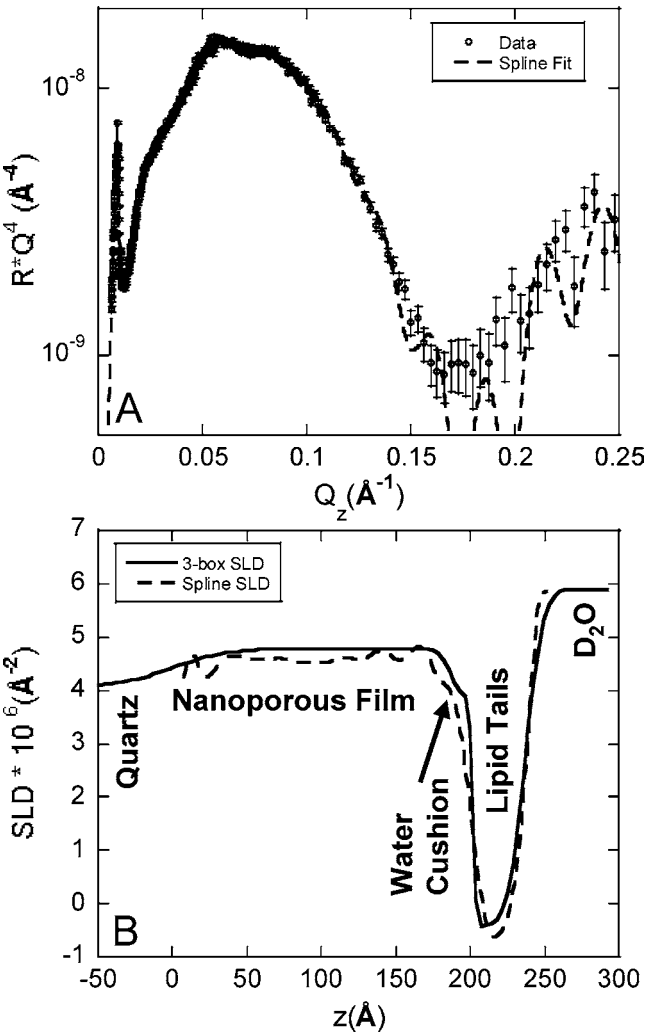

Figure 5. (A) Neutron reflectivity measured for a lipid bilayer on a nanoporous film and the model independent B-spline fit based on the SLD profiles shown in B. (B) Comparison between the three-box model and B-spline SLD profiles used for fits in Figures 4A and 5A, respectively.

where the three-box model describes a water cushion of 14.6 Å. Since the nanoporous film thickness is kept constant for the two models, the location of the average quartz−film interface is offset by approximately 12.6 Å for the three-box model. From the SLD of the nanoporous film we can calculate the fraction of the subphase in the pores; $\rho_{film} = \rho_{SiO_2}(1-\epsilon) + \rho_{subphase}(\epsilon)$, where ϵ is the volume fraction occupied by the subphase. The value of $\epsilon = 0.54$ is consistent with reported porosity from nitrogen porosimetry data on similar films.[32,33] The thickness of the hydrocarbon tails in the bilayer, $t_{\text{bilayer,HCtails}} = 35.3$ Å is higher than the previous case and corresponds to area per unit molecule of 37 ± 5 Å^2. As with a lipid membrane on the ordered nanocomposite film the SLD, $(-0.40 \pm 0.05) \times 10^{-6}$ Å^{-2}, of the single lipid bilayer is consistent with a well-packed membrane. The combined thickness of the water cushion and the hydrated headgroups of 14.6 Å is consistent with values reported in the literature.[1,22,23,54]

Figure 5a shows the cubic B-spline fit obtained for data in Figure 4a with parameters $\beta = 1.5$, $n = 40$, $d = 250$, and weights, $w_1 = 0.5$ and $w_2 = 0.5$. Since the model independent fitting routine is independent of any a priori knowledge or input of the SLD profile, comparing the thickness of the lipid tails (200 Å $< z <$ 250 Å) and the feature due to the presence of the water cushion (175 Å $< z <$ 200 Å) to the three-box model SLD profile (Figure 5b) supports the rationale of using the three-box model and the values obtained.

Conclusions

We have used neutron reflectivity to demonstrate that continuous, uniform, and stable supported bilayer membranes are formed over large areas (hundreds of mm^2) of ordered nanocomposite and nanoporous silica films. In contrast to nanoporous alumina supports, these films do not require surface treatments prior to lipid bilayer deposition. Furthermore, our results show that (1) the slightly hydrophobic nanocomposite film surface (water contact angle = 40°) allows for the facile assembly of a well-packed lipid bilayer and (2) a thicker/stretched (by 2 Å) zwitterionic lipid POPC membrane self-assembles well onto hydrophilic positively charged nanoporous films (note that for nanoporous films pH = 2* < isoelectric point < pH ≈ 4). NR estimates the thickness of the hydrocarbon tails in fluid POPC bilayers at 35.3 Å and the hydration layer between the tails and support at 14.6 Å on the nanoporous film. The hydration layer between the nanocomposite film and the lipid membrane is not discernible due to lack of contrast. The topography, porosity, and surface chemistry of these nanoporous and nanocomposite films may be contributing to the efficacy of membrane deposition. In our case the surface charge density for the nanoporous film is low due to the close proximity of the isoelectric point (compared to when in a phosphate buffer saline, pH ≈ 7.4); however, we find the assembled fluid membrane thickness shows only a 10% decrease in thickness over values reported on charged surfaces[49,50] compared to about 50% decrease seen by Burgess et al.[25] for fluid DMPC/cholesterol bilayers on gold electrodes. Future experiments that tune the surface charge density (via change of subphase pH) and hydrophobicity (silane treatments) will address these issues further. This characterization study enables future sensor development using this novel membrane architecture where the nanoporous/nanocomposite film can act as a fluid reservoir for transport, to facilitate transmembrane protein incorporation, or as a selective barrier for electrochemical reactions.

Acknowledgment. We thank Professor Pedersen (University of Århus, Denmark) for providing us with the cubic B-spline fitting program, Dr. Hamilton (ORNL) for use of the MIRROR fitting program, and Dr. Braun (HMI-Berlin, Germany) for the Parratt32 reflectivity program. Dr. S. S. Dixit and Dr. C. K. Yee (UC-Davis) for assistance with FRAP measurements. The authors thank the LANL and SNL−LDRD program, and DOE Office of Science (Basic Energy Sciences) for financial support. D.A.D. acknowledges support from the LANL Director's Postdoctoral Fellowship. A.N.P. also acknowledges support from NSF through Center for Biophotonics Science and Technology managed by the University of California, Davis, under Cooperative Agreement No. PHY 0120999. C.J.B. acknowledges support from AFOSR and ARO. This work was supported by Los Alamos National Laboratory under DOE Contract W7405-ENG-36, and by the DOE Office of Basic Energy Science.

Supporting Information Available: FRAP studies of Texas Red DHPE in DLPC at pH 2. This material is available free of charge via the Internet at http://pubs.acs.org.

LA0471240